2D and 3D-ISAR Images of a Small Quadcopter

2D and 3D-ISAR Images of a Small Quadcopter

Massimiliano Pieraccini, Neda Rojhani, Lapo Miccinesi
Department of Information Engineering
University of Florence
Via Santa Marta, 3
Firenze, Italy

***Abstract*—In this paper Inverse Synthetic Aperture Radar (ISAR) technique has been applied for obtaining 2D and 3D radar images of a small quadcopter. The aim is to prove the capability of radar technology for 3D imaging small drone targets.**

Keywords— drone, inverse synthetic aperture radar, radar, unmanned aerial vehicles

I. INTRODUCTION

Currently, the increasing number of small flying unmanned aerial vehicles (UAV) pose a serious challenge for preventing them being used for terrorist attacks, espionage or other malicious activities against sites with critical infrastructures. Furthermore, they pose threat for the safety of flights [1] and, last but not least, UAVs flying in private area pose privacy concerns [2].

Radar appears the technology of choice for detecting them, so an accurate estimate of the radar signature of UAVs is of increasing interest [3]-[6]. The acronym ISAR (Inverse Synthetic Aperture Radar) refers to an image processing that exploits the motion of the target instead of the motion of the radar [7]. More properly, it refers to the case when the measurement geometry is not *a-priori* known and it is obtained by the acquired data. Nevertheless, the same term is used more and more frequently even when the geometry is perfectly known [3],[6]. With reference to latter meaning, we state that the aim of this paper is to synthesize high resolution ISAR images of a small professional quadcopter. Although in a real application the effects the rotation of blades should be considered [8,9], in this preliminary study the blades will be assumed not rotating.

As it is well-known, ISAR algorithms are able to synthesize a high resolution image of target [10]-[14]. Unfortunately the side lobes of the point spread function (PSF) can affect heavily the ISAR image. For reducing them an incoherent summation of the ISAR images relative to 4 arcs of 180° has been performed with good results.

II. THE MEASUREMENT EQUIPMENT

A sketch of the measurement equipment is shown in Figure 1. A VNA (HP 8720A) operates as Continuous Wave Step Frequency (CWSF) transceiver. It is linked through microwave cables to a radar front-end held on a tripod.

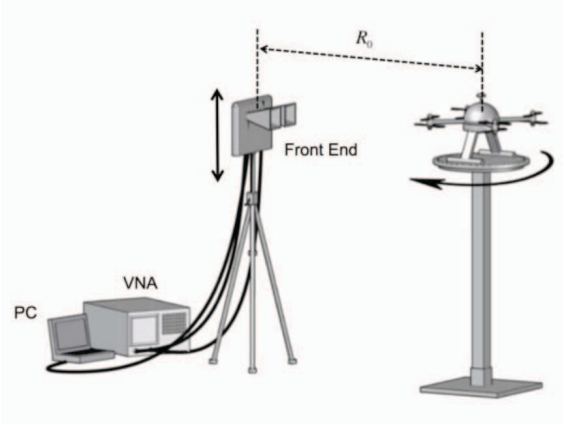

Fig. 1. Sketch of the measurement equipmemnt

The front-end (see Fig. 2) consists of a TX amplifier with a gain of 10 dB, a RX amplifier with a gain of 20 dB, and a pair of single-pole double-throw (SPDT) switches that provide a direct path (through a -40 dB attenuator) between the transmitter and the receiver in order to perform calibrated measurements not affected by the movements of the cables. The antennas are two equal horns linearly polarized, with rectangular aperture 5.5 cm × 7.5 cm, designed for operating in the band 8-12 GHz. A Band Pass Filter in the same band defines the noise bandwidth. The front-end can be rotated for obtaining measurements both in vertical and in horizontal polarization. Finally a Low Pass Filter at the end of the receiver chain cuts possible harmonic frequencies that amplifiers can introduce.

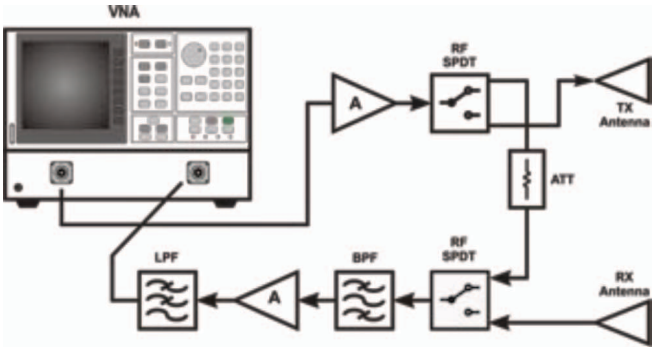

Fig. 2. Block scheme of the radar front-end

III. THE UAV UNDER TEST

As representative professional UAV we selected a NT4Contras quadcopter, manufactured by AirVision (Fig. 3). It has 4 pairs of engines with counter-rotating blades. The frame is carbon. It is powered by two 4600 mAh Li-Poli batteries housed in the legs. Below the head there is a dock for a camera which is not provided. The distance from the engines is 38 cm. The height of the motors from ground is 22 cm.

Fig. 3. Quadcopter under test

IV. ISAR PROCESSING

The basic idea of ISAR is to exploit the spatial diversity of data acquired for focusing a high resolution image. Using the equipment described above, and shifting step by step along z the height of the radar head, the result of a measurement session is a matrix $N_f \times N_p \times N_z$ of complex numbers:

$$E_{i,k,m} = I_{i,k,m} + jQ_{i,k,m} \tag{1}$$

where $I_{i,k}$ and $Q_{i,k}$ are the in-phase and the quadrature components acquired at i-th frequency ($1<i<N_f$), at the k-th angular position ($1<k<N_p$), and at m-th height ($1<k<N_z$). With reference to Fig. 4, the basic formula for focusing in a generic point identified by the coordinate (x,y,z) is [15]:

$$I(x,y,z) = \sum_{i,k,m} E_{i,k} e^{j\frac{4\pi}{c} f_i R_{k,m}(x,y,z)} \tag{2}$$

where $R_{k,m}(x,y,z)$ is the distance between the image-point (x,y,z) and the position identified by the indexes k and m.

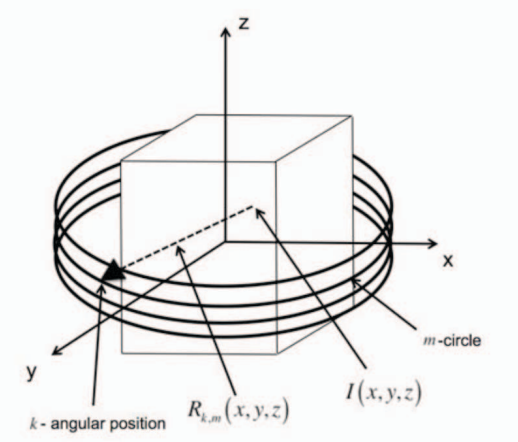

Fig. 4. ISAR geometry

V. CROSS-RANGE WINDOWING

Fig. 5 shows the basic idea of the windowing procedure we applied. The rotation circle is divided in 4 arcs of 180° (for maintaining the highest possible resolution) partially overlapping.

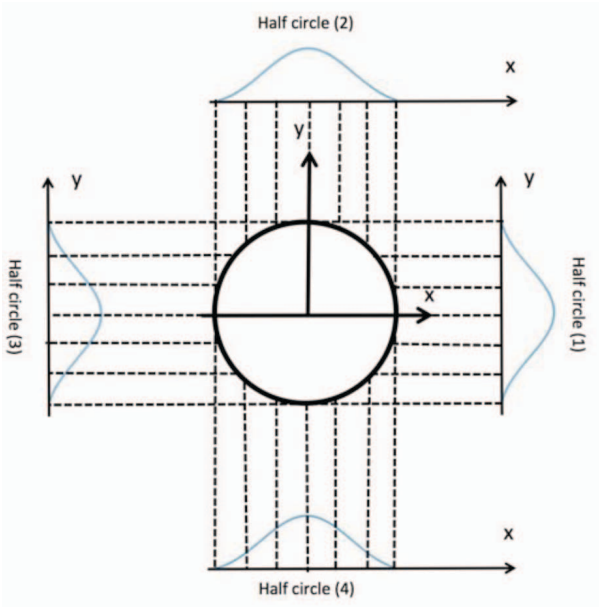

Fig. 5. Windowing procedure

Before focusing, at each arc is applied a window projected on the chord subtended to the same arc. If the arcs are disposed as in Fig. 5 the chords are parallel to the x and y axes. The ISAR algorithm is applied to each arc separately and the obtained images $I(x,y,z)$ are summed incoherently, i.e. discharging the phase:

$$I_w(x,y,z) = |I_1(x,y,z)| + |I_2(x,y,z)| + |I_3(x,y,z)| + |I_4(x,y,z)| \tag{3}$$

The Point Spread Function (PSF) of a single point using the procedure described above is shown in Fig. 6. The blue line is the PSF calculated without any angular windowing. The red line is the PSF with 4 windows applied as described above. The green line is the PSF using 8 windows, i.e. by dividing the

circle in 8 arcs of 180° partially overlapping. The later is a bit better (a bit lower in the sides) than the red line (4 windows), but the advantage appears marginal, by considering that the computational cost doubles. It is of note that even the PSF with 16 windows has been calculated, but it has resulted quite indistinguishable from the PSF with 8 windows.

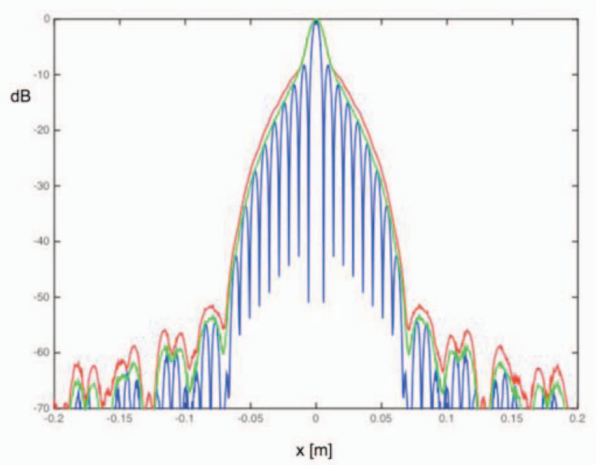

Fig. 6. PSF with no window (blue line), with 4 windows (red line), and with 8 windows (green line)

Fig. 7 shows the obtained ISAR image of the UAV in Fig. 3 without application of the 4 windows. The typical ripple due to the cross-range lobes is evident. Fig. 8 shows the image obtained with windowing. Its quality appears better.

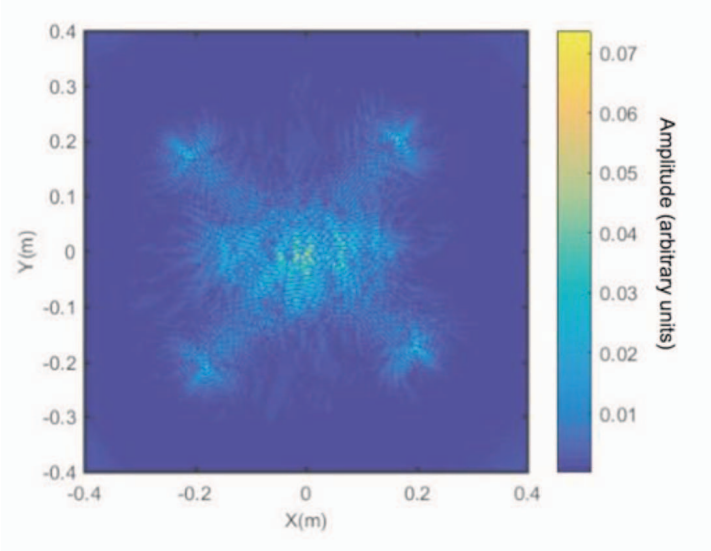

Fig. 7. 2D-ISAR image of the UAV in Fig. 3

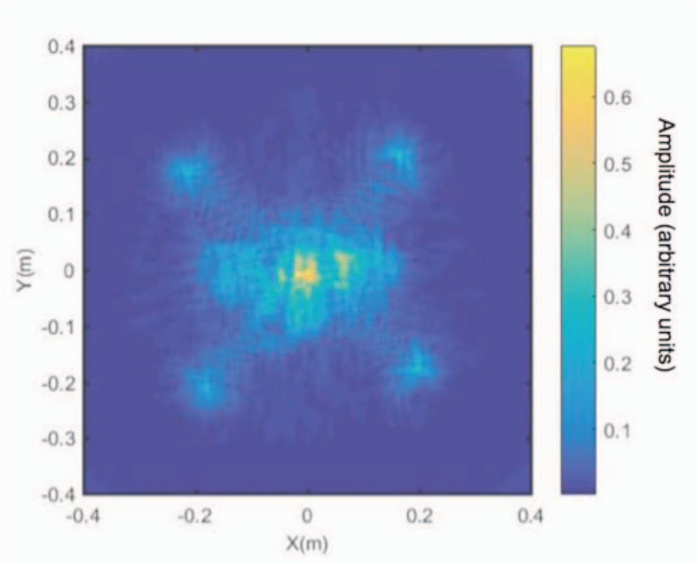

Fig. 8. 2D-ISAR image of the UAV in Fig. 3 using the windowing procedure

VI. 3D ISAR IMAGES

The ISAR algorithm can be used even for retrieving 3D images (provided a further movement of the radar head in vertical direction). Fig. 9 and Fig. 10 show two views of the 3D image obtained with and without cross-range windowing.

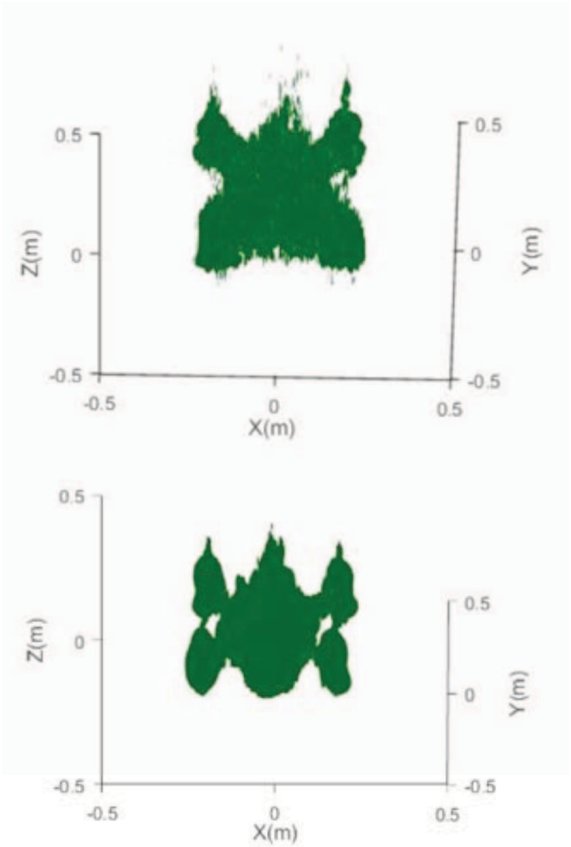

Fig. 9. Views of the 3D-ISAR image of the UAV. The upper image is without windowing, while the lower is with windowing

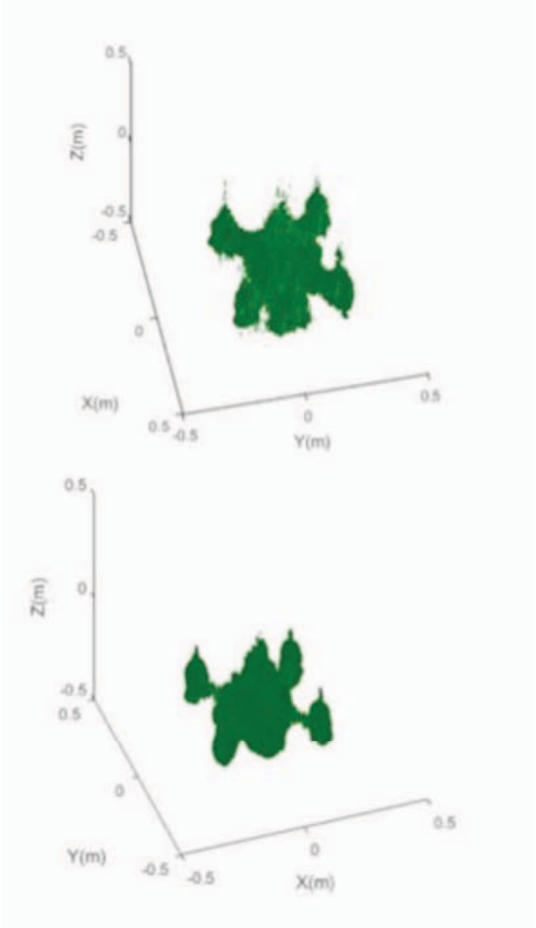

Fig. 10. Views of the 3D-ISAR image of the UAV. The upper image is without windowing, while the lower is with windowing

VII. CONCLUSION

ISAR technique has been proven to provide detailed 2D and 3D images of small drones. The next steps should be obtain them with non-cooperative targets. This is a very challenging objective as the rotation of blades could heavily blurry the images if it is not taken into account in focusing algorithm.

REFERENCES

[1] CNN, http://edition.cnn.com/2015/10/07/politics/faa-anti-drone-technology/ (October 8, 2015)

[2] The New York Times, http://www.nytimes.com/2016/01/10/opinion/sunday/drone-regulations-should-focus-on-safety-and-privacy.html?_r=0 (January 9, 2016)

[3] L. To, A. Bati, D. Hilliard, “Radar Cross Section measurements of small Unmanned Air Vehicle Systems in non-cooperative field environments.” In 2009 3rd European Conference on Antennas and Propagation (pp. 3637-3641). IEEE. March 2009

[4] N. Altin and E. Yazgan The Calculation of Back Scattering Field of Unmanned Air Vehicle, PIERS Proceedings, Beijing, China, March 23–27, 2009, pp. 1460-1463

[5] M. A Ritchie, F. Fioranelli, H. Griffith, B. Torvik, “Micro-drone RCS analysis”, International conference on RADAR, Johannesburg, South Africa, October 2015

[6] C. Li, H. Ling, "An Investigation on the Radar Signatures of Small Consumer Drones," IEEE Antennas and Wireless Propagation Letters vol. 16, pp.649-652, 2017

[7] V. C. Chen, M. Martorella “Inverse Synthetic Aperture Radar Imaging: Principles, Algorithms, and Applications” SciTech Publishing, 2014

[8] H. T. Tran, R. Melino, P. E. Berry and D. Yau, “Microwave radar imaging of rotating blades.” 2013 International Conference on Radar, Adelaide, SA, 2013, pp. 202-20

[9] F. Fioranelli, M. Ritchie, H. Griffiths, and H. Borrion, “Classification of loaded/unloaded micro-drones using multistatic radar,” Electron. Lett., vol. 51, no. 22, pp. 1813–1815, 2015.

[10] J. Fortuny, “An efficient 3-D near-field ISAR algorithm”. IEEE Transactions on Aerospace and Electronic Systems, Vol. 34 No. 4, pp. 1261-1270 (1998)

[11] J.T. Mayhan, M.L. Burrows, K.M. Cuomo, J.E. Piou. “High resolution 3D “snapshot” ISAR imaging and feature extraction.” IEEE transactions on aerospace and electronic systems, Vol. 37, No. 2, pp. 630-642 (2001)

[12] K.E. Dungan, L.C. Potter, L. C. “3-D imaging of vehicles using wide aperture radar.” IEEE Transactions on Aerospace and Electronic Systems, 47(1), 187-200 (2011)

[13] D. L. Mensa, High Resolution Radar Cross-Section Imaging, 2nd ed., Artech House, 1991

[14] T. Sakamoto, T. Sato, P. Aubry, A. Yarovoy , “Fast imaging method for security systems using ultrawideband radar”. IEEE Transactions on Aerospace and Electronic Systems, Vol. 52 No. 2, pp. 658-670 (2016)

[15] M. Pieraccini, N. Agostini, F. Papi, S. Rocchio. “A rotating antenna ground-based SAR”. In 2015 IEEE European Microwave Conference (EuMC), pp. 1515-1518 (2015)